Arch. Metall. Mater. **70** (2025), 4, 1945-1953

DOI: https://doi.org/10.24425/amm.2025.156281

QINGXIAO ZHANG[1], XIAOHUA WEI[1*], YINJIAN MA[2,3], QING YUAN[2*]

EFFECT OF COILING TEMPERATURE ON THE MICROSTRUCTURE AND STRENGTH CONTRIBUTION IN ONE NOVEL Fe-1.5Al-2Mn-0.18C AUTOMOBILE STEEL

An automobile steel with density of 7.55 g/cm^3 and composition consisting of Fe-1.5Al-2Mn-0.18C was successfully produced, exhibiting remarkable tensile strength of 897.7 MPa and ductility of 19.3%. This steel's microstructural transformations and their contributions to strength were analyzed after undergoing coiling treatments at temperatures of 400°C, 500°C, and 600°C. Our findings reveal an inverse relationship between the coiling temperature and both the steel's strength and the product of strength and elongation (PSE), whereas ductility shows a positive correlation with rising coiling temperatures. The primary factors accounting for these variations in strength across different coiling temperatures are phase transformation strengthening, grain refinement strengthening, dislocation strengthening, and precipitation strengthening, with phase transformation and dislocation strengthening being the most influential. Furthermore, the reduction in size and volume fraction of (Ti, V)C particles observed at lower coiling temperatures is attributed to differences in carbide ripening and nucleation processes. In conclusion, this optimized low Mn-Al alloy chemistry combined with a hot rolling process provided a novel method to produce the automobile with low density and acceptable mechanical properties.

Keywords: Automobile steel; microstructure; mechanical property; dislocation; carbides

1. Introduction

To improve fuel efficiency and reduce the carbon emission as much as possible, the automotive industry has been working hard to reduce the weight of vehicles themselves [1-2]. The two main ways to reduce the body weight in automobiles to realize lightweight include structure design and application of low-density high-strength materials [3-4]. In all fairness it must be admitted that there is limited enough expanding space for the optimization in body structure of automobiles. Therefore, the application of low-density high-strength materials become the mainstream choice in lightweight automobiles [5-8]. There have been many lightweight materials such as aluminum alloy, magnesium alloy and composite materials are employed in the lightweight automobiles [9-10]. However, some of them are limited in industrial production due to its complex technology and precious alloys. High-strength steel with low-density are prevalent to satisfy the lightweight requirement due to its mass-production techniques and low alloy cost [11-12]. The prominent advantage in lightweight high-strength steel has manifested the future development direction in automobiles, especially for the electric vehicle. Therefore, research on the lightweight high-strength steel have been one hot research topic.

Fe-Mn-Al-C series lightweight high-strength steel by adding many lightweight elements such as Mn, Al to achieve the reducing density and weight, gradually become one of the main types of lightweight steel in the future [13-15]. This kind of steel has both high strength and good toughness-plasticity. However, the existing literature about the Fe-Mn-Al-C series lightweight high-strength steel are mainly focused on the moderate or high Mn and Al content steels. For example, Peng et al. investigated the relationship between the microstructure evolution and mechanical properties in one developed Fe-10Mn-5.5Al-0.25C steel, and found that the soaking temperature decided the main mechanical performance in this austenitic lightweight steel [16]. Lee et al. studied the influence of precipitated k-carbide on the Fe-9Mn-6Al-0.15C steel and declared that the k-carbide at the boundaries precipitated before the eutectoid precipitation during the isothermal aging [17]. Another Fe-11Mn-2/4Al-0.2C lightweight steel was fabricated in the research of Ding et al., and it shew the excellent strength-ductility balance attributed by the newly formed martensite. Besides, it also demonstrated

[1] SCHOOL OF MECHATRONIC ENGINEERING, QUZHOU COLLEGE OF TECHNOLOGY, QUZHOU 324000, CHINA
[2] WUHAN UNIVERSITY OF SCIENCE AND TECHNOLOGY, STATE KEY LABORATORY OF REFRACTORIES AND METALLURGY WUHAN 430081, CHINA
[3] ZHEJIANG SUNHI-MACH CO., LTD, CHINA

* Corresponding authors:1456046192@qq.com, yuanqing@wust.edu.cn

the decreased ultimate tensile strength and increased elongation by more Al addition [18]. The strain hardening behavior during plastic deformation in a Fe-12Mn-8Al-0.8C lightweight steel was reported in the research of Ding et al., and they clarified that the multiple-stage stain hardening contributed the steady strain hardening behavior [19].

The common characteristic in these investigations are the outstanding mechanical properties introduced by multiple strengthening mechanisms in Fe-Mn-Al-C series lightweight high-strength steel. However, because the alloy ratio of Mn and Al in these steels are much higher than that of conventional steel, the alloy cost is unquestionable high. More importantly, the interaction between the high Mn or/and high Al molten steel and the refractory materials (ladle and tundish), and the molten slag (continuous casting protection slag, refining slag, tundish covering agent) during the smelting and casting processes are far more complicated than the those in conventional steel. The molten steel is easy to bond with the lining or the protective slag, which causes difficulties in continuous casting, affects the production rhythm, and then destroys the ladle structure. Consequently, the difficulty of industrial production of low-density high-strength steel was greatly improved. Thus it can be seen that the most investigated Fe-Mn-Al-C series lightweight high-strength steel are not suitable for industrial production until now.

One novel Fe-1.5Al-2Mn-0.18C automotive steel with a density of 7.55 g/cm³ suitable for hot-rolling technological process was developed in current work to attempt the decreased density and industrial production. The microstructure evolution and strength contribution under different coiling temperatures were elaborated discussed. Results will provide process guidance for the hot rolling parameters of Fe-1.5Al-2Mn-0.18C automotive steel.

2. Materials and experimental methods

The experimental steel with chemical composition of Fe-1.5Al-2Mn-0.18C-0.7Si-0.25Ni-0.16 (Ti+V)-0.010P-0.003S was smelted and hot-rolled in one pilot plant. The density of this experimental steel was measured to be 7.55 g/cm^3 using water level method which was greater than the critical density value of low-density steel of 7.2 g/cm^3 [20]. The heating temperature and holding time before hot rolling were 1250°C and 2 h, respectively. The hot rolling with 1050~1150°C initial rolling temperature and 860°C finishing rolling temperature were carried out in succession after soaking. The hot rolling was finished on an 800 hot-rolling reverse mill with a diameter of 850 mm rolling mill (maximum rolling force = 800 KN), and the rolling speed was about 2.8 m/s. About eight successive passes were applied in the finishing rolling stage. Subsequently, one rolling plate with 14 mm thickness (the total rolling deformation was about 85%) and 177 mm width was obtained after laminar cooling. Fig. 1 shows the thermal simulation process with different coiling temperatures. The precision-machined specimens whose lengthwise direction was parallel to the slab rolling direction (RD) presented by Fig. 2a were obtained for the thermal simulation tests. Firstly, the specimen was reheated to 1200°C in a heating rate of 10°C/s and then isothermal held for 5 min. Subsequently, the specimen was cooled to the designed rough rolling temperature of 1150°C and finishing rolling temperature of 860°C with the same cooling rate of 10°C/s. 50% reduction and 30% reduction which simulated the rough and finishing rolling process shown by Fig. 1 were carried out during the simulation rough and finishing rolling stages, and the reduction rates were 5 s^{-1} and 10 s^{-1}, respectively. The cooling rate of 40°C/s was employed after finishing rolling followed by coiling to stimulate the laminar cooling. The coiling stage was held for 30 min with temperatures of 400, 500 and 600°C. And then the specimen was finally cooled to room temperature with 5°C/s. All the used hot rolling parameters were to simulate the industrial production process as clear as possible.

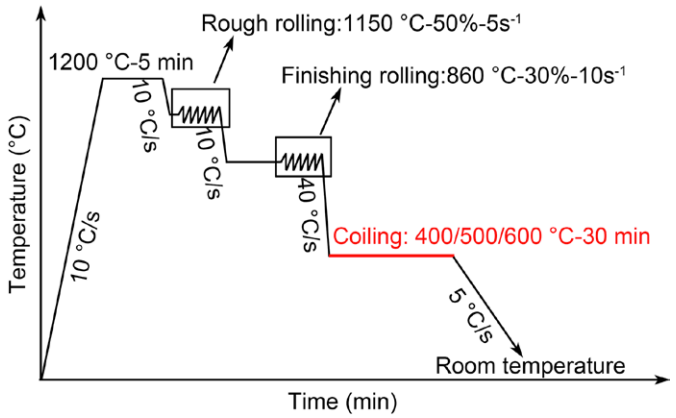

Fig. 1. Schematic diagram for hot-rolling process with different coiling temperatures in experimental steel

The dimension of specimen for above thermal simulation test is shown in Fig. 2a. To determine the tensile properties of these thermal simulation specimens with different coiling temperatures, the miniature bone-like tensile specimen illustrated by Fig. 2b was machined from the reduction area in Fig. 2a. The

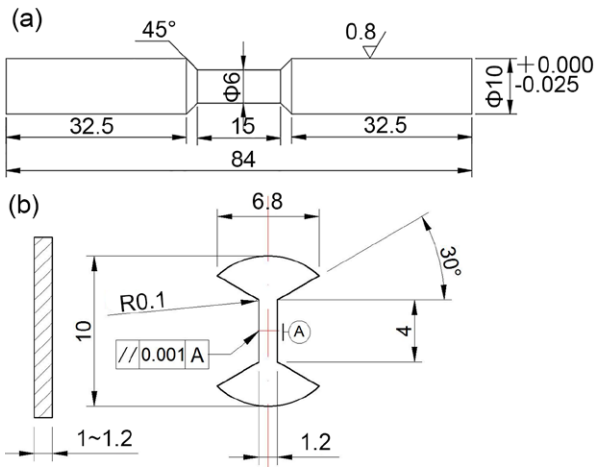

Fig. 2. Specimens dimension for (a) hot-rolling experiments and (b) subsequent tensile tests

axial direction of tensile specimen was parallel to the normal direction (ND) of the experimental steel. Therefore, the obtained tensile properties manifested the immediate comparing of tensile properties in ND between specimens coiled at different temperatures. It should be noted that similar methods were adopted in many experiments, and some literature showed that the influence of rolling direction on the properties could be ignored [21-23].

Microstructural characterizations were conducted utilizing advanced techniques, including light microscopy (ZEISS) and field emission scanning electron microscopy (FE-SEM, Nova 400 Nano), to provide detailed insights into the microstructural features. To further elaborate on the subtle differences in microstructure, electron backscatter diffraction (EBSD) analysis was performed. Additionally, transmission electron microscopy (TEM, JEM-2100UHR), equipped with an energy-dispersive spectrometer (INCA-EDS), was employed to analyze precipitates within carbon replica specimens, enabling a comprehensive understanding of their composition and distribution. The size of precipitates was determined by Nano Measure software based on more than 50 precipitates. And the density of precipitates was estimated using Image-Pro Plus software. Enough precipitates were counted to ensure the measure accuracy [24].

3. Results and discussions

3.1. Mechanical property

Fig. 3 presents the mechanical properties of specimens coiled at different temperatures. The tensile properties parallel to ND in as-hot rolled specimen are given as one counterpart. The as-hot rolled specimen had the greatest strength (yield strength: 873.0 MPa, tensile strength: 1072.1 MPa) but the worst ductility of 7.5%. The strength all decreased in the specimens coiled at 400~600°C while the ductility was substantially improved. The yield strength decreased from 780.1 MPa to 738.2 MPa and then 648.9 MPa with the increased coiled temperature from 400 to 600°C, and then tensile strength decreased as well from 897.7 MPa to 822.1 MPa and then 758.5 MPa. Conversely, the ductility increased from 19.3% to 20.7% and then 21.5% with the increased coiling temperature. The optimal balance was achieved in the specimen coiled at 400°C, exhibiting the highest product of strength and elongation (PSE) at 17.35 GPa·%. Subsequently, a slight decrease in PSE was observed with the escalation of coiling temperature. Notably, compared to the as-hot rolled specimen, significant enhancements in ductility and PSE were achieved, albeit with a minor compromise in strength. Compared to some reported low-density steels in different chemical compositions, such as Fe-12.6Mn-9Al-0.8C-0.6Si-0.2Ni (σ_s = 702 MPa, A = 14.2%) [25], Fe-0.16C-0.83Mn-0.056Si-1.8Al-0.075P-0.22Cr-0.027Nb (σ_s = 540 MPa, A = 15.04%)[26], Fe-3.5Mn-5.8Al-0.3C (σ_s = 532 MPa, A = 23.2%) [27], the developed automobile steel in current work signified obvious dominance in the chemical composition and the mechanical properties. Compared to the commercial TRIP steel with similar chemical composition, it was found that the developed steel had a higher yield strength and similar total elongation. Furthermore, the fabrication method in the developed automobile steel was plainer without the high-temperature annealing mentioned by L. Kucerova [28]. In other TRIP steels, the Al content was designed as 1.5 wt.%, however, most steels used medium-Mn content to realize the best mechanical performance [29-30]. Thus it can be seen that the developed automobile steel with good mechanical properties and decreased density are promising in future industrial production.

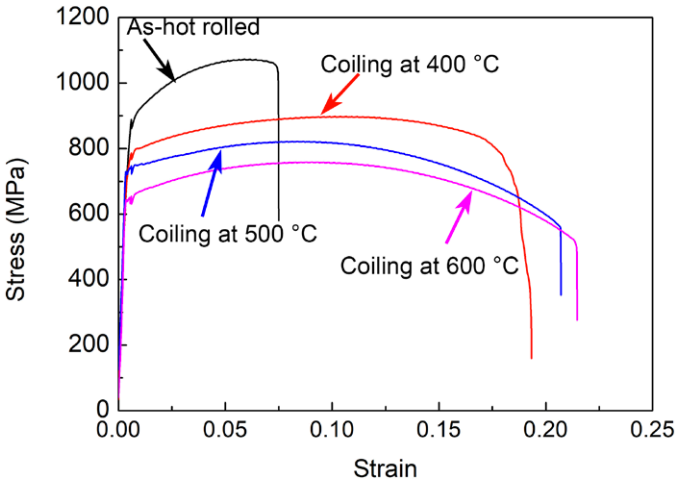

Fig. 3. Tensile properties for as-hot rolled specimen and three specimens coiled at 400, 500 and 600°C

3.2. Microstructure

The OM images in specimens are given in Fig. 4. Apparent microstructure segregation was found in the as-hot rolled specimen. The bainite/martensite (B+M) banding in dark brown was separated by the banding light ferrite (F). The microstructure segregation disappeared in the re-hot rolled specimens coiled at different temperatures. The B+M was dominating in the specimen coiled at 400°C, and the volume fraction of B+M was obviously decreased with the increase of coiling temperature (500°C). The partial B+M was replaced by pearlite (P) when coiling temperature of 600°C was applied, and the volume fraction of polygonal F increased apparently.

Fig. 5 exhibits the SEM images representing the microstructures in above specimens. The mixture microstructures of B+M was clear in the as-hot rolled specimen. And the mixture microstructures of B+M became more and more inconspicuous with the increase of coiling temperature. Inversely, the polygonal F was popular with the increasing coiling temperature. Therefore, it can be found that the decreased strength was primarily caused by the different transformation from specimen coiled at 400°C to 600°C. The highest strength in the specimen coiled at 400°C was mainly attributed to the more volume fraction of martensite/bainite islands. And the lowest strength was caused by the more polygonal F.

The inverse pole figure (IPF) and grain boundary (GB) images for specimens coiled at 400°C and 600°C are presented

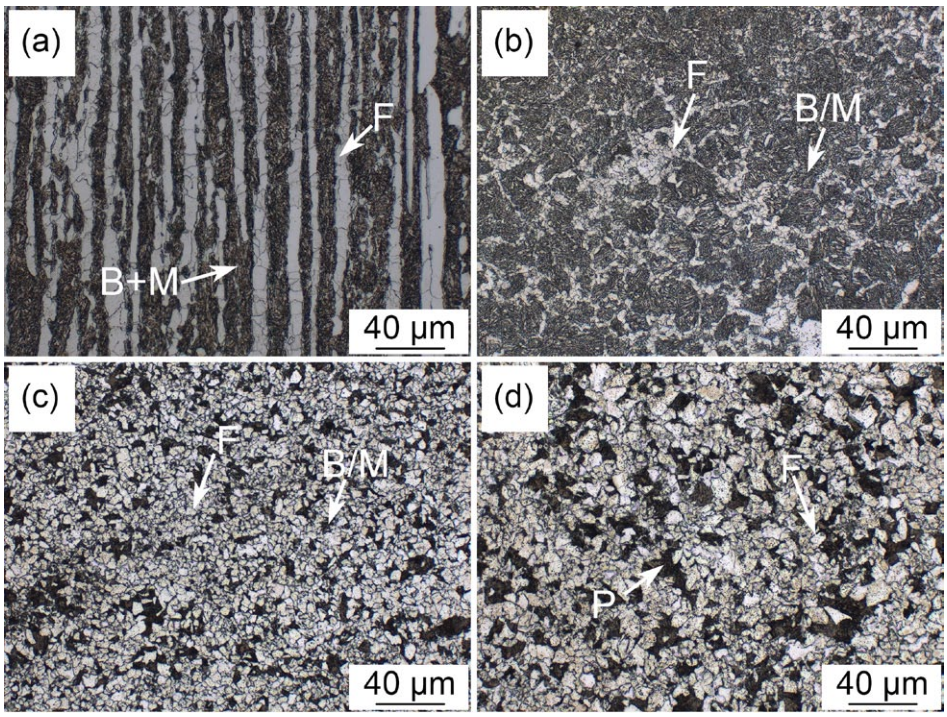

Fig. 4. Light microscopy images showing the microstructures of (a) as-hot rolled specimen and specimens coiled at (b) 400, (c) 500 and (d) 600℃

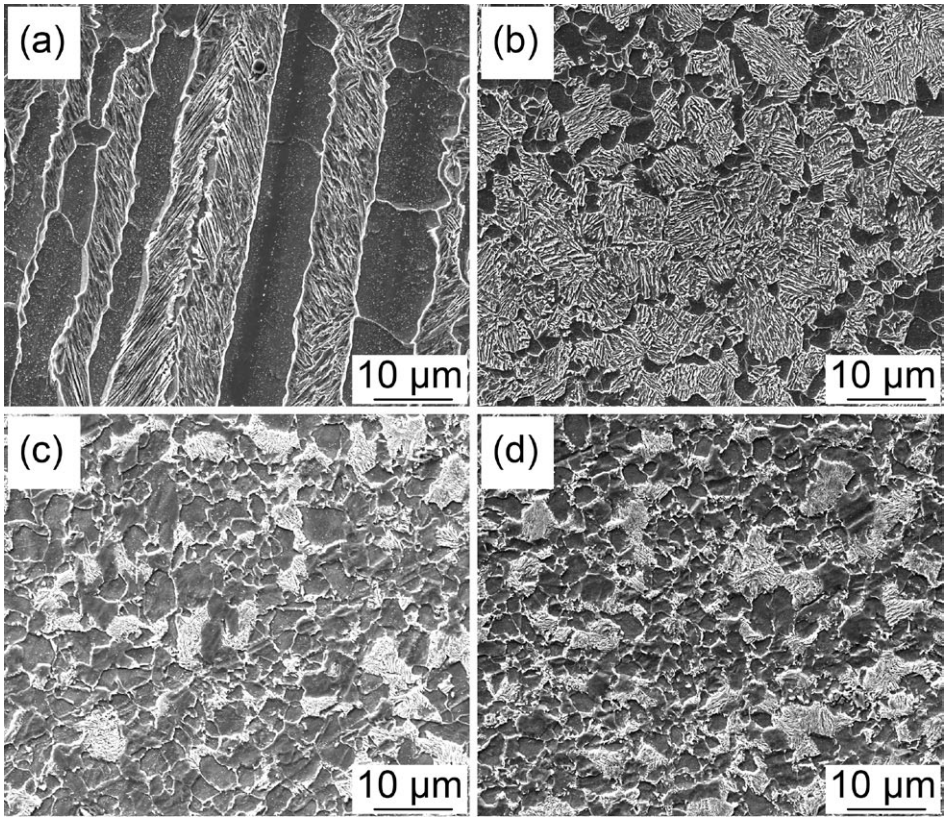

Fig. 5. SEM images showing the microstructures of (a) as-hot rolled specimen and specimens coiled at (b) 400, (c) 500 and (d) 600℃

in Fig. 6. Analysis revealed a notable difference in grain boundary distribution, with the 400°C coiled specimen containing 30.6% low-angle grain boundaries (LAGB, 2-10°) and 69.4% high-angle grain boundaries (HAGB, ≥10°). Conversely, the 600°C coiled specimen exhibited a decrease in LAGB to 16.0% and an increase in HAGB to 84.0%. It is understood that martensite, comprising a hierarchical structure of packets, blocks, and laths, primarily exhibits LAGB between martensite laths. Here, LAGB is associated with unit size, a key factor influencing strength, whereas HAGB (misorientation ≥10°) is pivotal in controlling

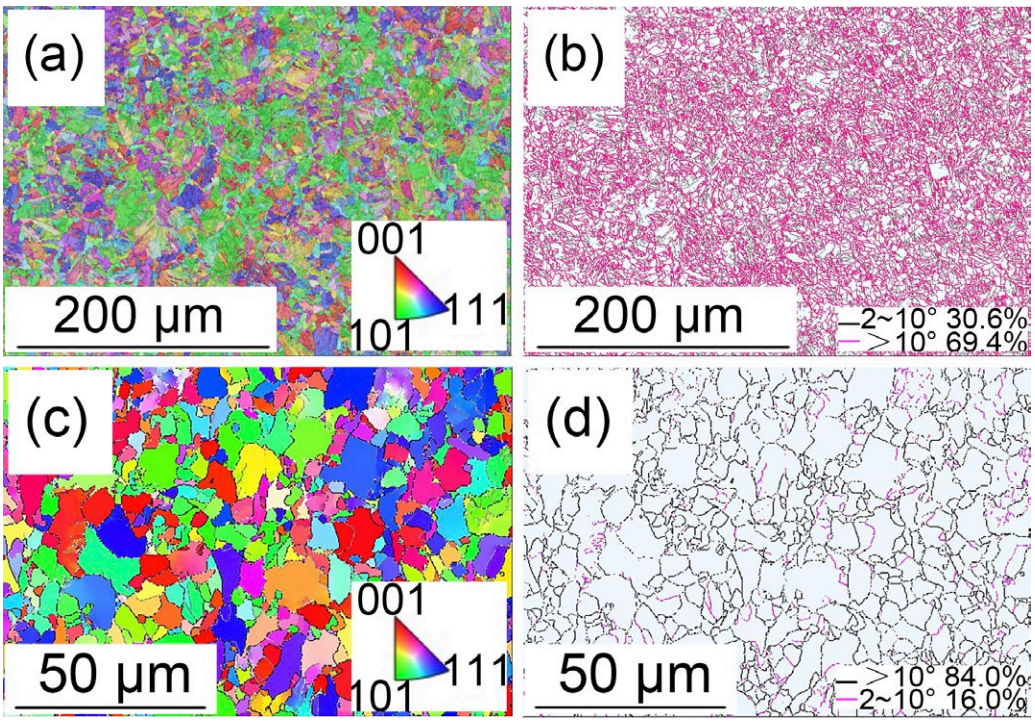

Fig. 6. IPF and GB images in the specimens coiled at (a, b) 400 and (c, d) 600°C

cleavage fracture processes. It is noted that interphase boundaries such as F/M, F/B and B/M in the set of grain boundaries were not considered because it was blurred when calculating the grain refinement contribution. The slightly elevated LAGB proportion introduced by the higher volume fraction of martensite in the 400°C coiled specimen underscores its relatively higher strength compared to the 600°C coiled counterpart. In addition, almost no apparent preferred orientation was found in the specimen coiled at 600°C. However, the green area showing the (101) orientation in specimen coiled at 400°C was apparent than those representing the (001) and (101) orientations. The slight (101) orientation in specimen coiled at 400°C was caused by the inheritance effect of microstructure segregation which was not fully evaded at low coiling temperature.

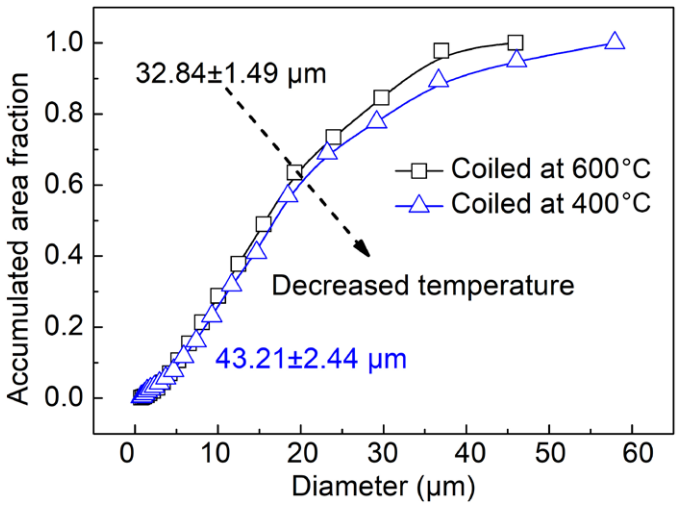

Fig. 7. Size distribution in the specimens coiled at 400 and 600°C

Fig. 7 illustrates the cumulative area fraction of martensite or ferrite diameters in specimens coiled at 400°C and 600°C. Applying the equivalent circular diameter method with a 10° criterion, the average diameter of martensite islands and ferrite grains in the 400°C coiled specimen was found to be 43.21±2.44 μm. Conversely, the grain size in the 600°C coiled specimen decreased to approximately 32.84±1.49 μm. This observation underscores the trend of decreasing grain size with an increase in coiling temperature, accompanied by a microstructural transformation from martensite to ferrite. The reduction in ferrite grain size can be attributed to the progressive recovery and recrystallization of martensite laths at higher coiling temperatures. Hence, the increased grain size by lower coiling temperature affected the strength as well although the strength changed by the different phase transformations at different coiling temperatures.

3.3. Precipitation

The carbides morphologies and corresponding selected area electron diffraction and point energy spectrum in specimen coiled at 400°C are presented in Fig. 8. Ellipsoidal carbides identified as (Ti, V)C particles were easily found, in which the content of element Ti was dominating. Some carbides presented chain distribution morphology and some of them were in relatively large size. Compared to the ellipsoidal (Ti, V)C carbides in the specimen coiled at 600°C in Fig. 9, it found that more (Ti, V)C carbides formed at the higher coiling temperature. However, the size of (Ti, V)C carbides became larger in the specimen coiled at 600°C.

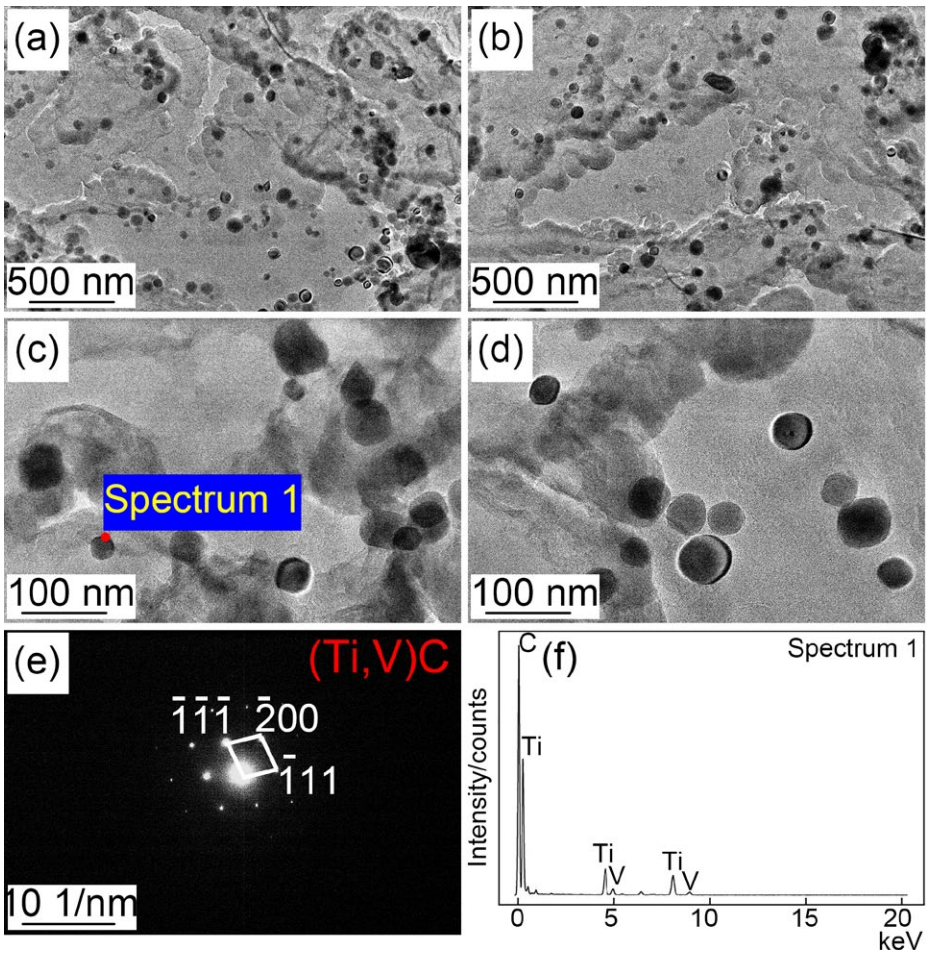

Fig. 8. (a-d) Precipitate morphology and corresponding (e) selected area electron diffraction spots and (f) point energy spectrum in the specimens coiled at 400℃

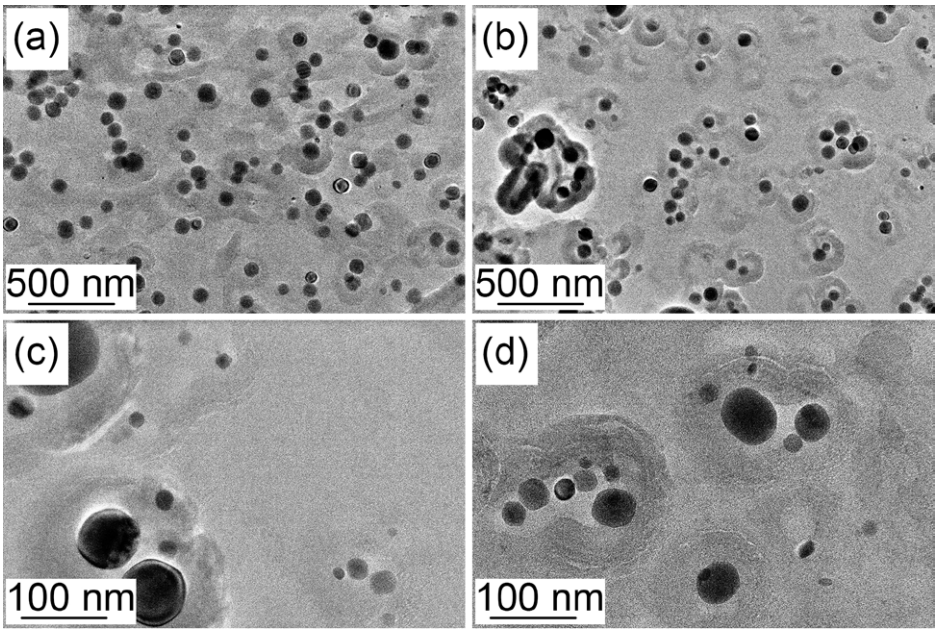

Fig. 9. Precipitate morphology in the specimens coiled at 600℃

Fig. 10 shows the size distribution of (Ti, V)C particles in specimens coiled at 400 and 600℃ based on Nano measurer and Image-Pro Plus software. Enough carbides were counted to ensure the measure accuracy. The average size of (Ti, V)C particles in specimen coiled at 400℃ was about 43.68 nm, which was relatively smaller than 49.69 nm in the specimen coiled at

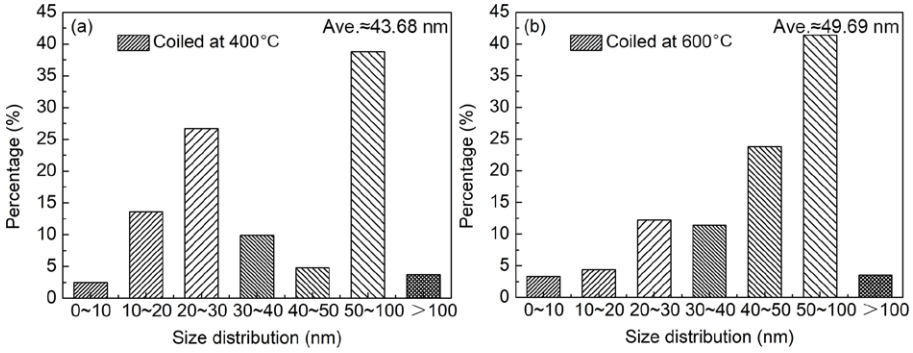

Fig. 10. Size distribution of (Ti, V)C particles in the specimens coiled at (a) 400 and (b) 600°C

600°C. The increased size was explained by the higher coiling temperature which facilitated the carbides ripening. Smaller carbides possess a higher concentration of carbon compared to their larger counterparts. Consequently, at elevated coiling temperatures, these smaller carbides become less stable, facilitating the migration of carbon atoms and leading to the coarsening of carbides. The volume fraction of (Ti, V)C particles in specimen coiled at 400°C was about 8.62%, which was lower than 11.17% in the specimen coiled at 600°C. The increased (Ti, V)C particles was ascribed to the higher coiling temperature which provided more driving force for carbides nucleation.

4. Strength contribution

It can be concluded from the above microstructure and carbides difference by different coiling temperature that the coiling temperature resulted in the different microstructure and carbides distribution. The martensite was obtained in a lower coiling temperature accompanied by the relatively smaller carbides, while more small-sized ferrite grains accompanied with large carbides were realized at higher coiling temperature. In order to provide better parameter guidance for the practical production of this automobile steel, the relationship between the coiling temperature and the strength contribution is crucial. And the clarification of the strength contribution in the investigated steel contributes to a clearer understanding of the precise regulation of process-microstructure-mechanical properties. However, there is a paucity of research that quantitatively examines the various strengthening mechanisms contributing to the strength of automobile steels with decreased density coiled at diverse temperatures. Typically, the yield strength of steel encompasses several components, including crystal lattice strengthening (σ_0), solid solution strengthening (($\Delta\sigma_s$), grain refinement strengthening ($\Delta\sigma_g$)), precipitation strengthening ($\Delta\sigma_p$), dislocation strengthening ($\Delta\sigma_d$), and phase transformation strengthening ($\Delta\sigma_{tran}$), as encapsulated in Eq. (1) [31].

$$\sigma = \sigma_0 + \Delta\sigma_s + \Delta\sigma_g + \Delta\sigma_p + \Delta\sigma_d + \Delta\sigma_{tran} \quad (1)$$

It is important to note that the contribution of crystal lattice strengthening in high strength steel has been determined to be approximately 48 MPa, while the estimated phase transformation strengthening, occurring during the formation of martensite, is 54.8 MPa.

The solid solution strengthening was evaluated using Eq. (2), where [X] denotes the mass fraction of an element present in the steel. The predominant precipitated particles in the developed automobile steel were primarily (Ti, V)C. Assuming that carbon is fully dissolved in the matrix and the remaining carbon is mostly present in carbides, the solid solution strengthening effect of carbon was calculated based on its maximum solubility. Nearly all nitrogen (N) in the steel precipitated as TiN, hence the solid solution strengthening contribution of N was disregarded. The alloying elements Si and Mn, being ferrite-forming elements, were considered to be dissolved in the ferritic matrix. Consequently, the calculated solution strengthening value ($\Delta\sigma_s$) for the developed automobile steels coiled at 400°C and 600°C was 96.68 MPa.

$$\Delta\sigma_s = 4570[\mathrm{C}] + 3750[\mathrm{N}] + 37[\mathrm{Mn}] + \\ + 83[\mathrm{Si}] + 80.5[\mathrm{Ti}] + 2.9[\mathrm{V}] - 30[\mathrm{Cr}] \quad (2)$$

The grain refinement strengthening was approximately estimated using the Hall-Petch relationship, as expressed in Eq. (3), where K is a constant (0.55 MPa · m$^{-1/2}$) and d represents the average grain size (in meters). The average grain size for the specimen coiled at 400°C was derived from the measurements presented in Fig. 6. Based on these calculations, the grain refinement strengthening values for the developed automobile steels coiled at 400°C and 600°C were determined to be 83.67 MPa and 95.97 MPa, respectively.

$$\Delta\sigma_g = Kd^{-\frac{1}{2}} \quad (3)$$

When calculating the dislocation strengthening, both the average Kernel Average Misorientation (KAM, θ) and the first boundary condition were taken into consideration. Fig. 11 displays the KAM distributions in the specimens coiled at 400 and 600°C. Very apparent dislocation accumulation was found in the specimen coiled at 400°C, while only small amount dislocation accumulation was captured along the grain boundaries of ferrite in the specimen coiled at 600°C. The more dislocation accumulation in the specimen coiled at 400°C was caused by the martensite islands and the inadequate defects recovery. The dis-

location density (ρ) was quantitatively determined using Eq. (4). Subsequently, the contribution of dislocation strengthening was evaluated by applying Eq. (5) [32-34].

$$\rho = \frac{\alpha\theta}{\mu b} \tag{4}$$

$$\Delta\sigma_\rho = \alpha M G b \rho^{\frac{1}{2}} \tag{5}$$

Here, α represents the dislocation strengthening factor (0.38), M is the average Taylor factor (2.75), G denotes the shear modulus (81600 MPa), b is the Burgers vector (2.48×10^{-10} m), and μ is the step size (0.5 μm). Based on these parameters, the estimated dislocation strengthening values for the specimens coiled at 400 and 600°C were 114.72 MPa and 185.86 MPa, respectively.

Precipitation strengthening value is evaluated by Ashby-Orowan Eq. (6) assuming the bypassing interactions between the carbides and dislocation. f and d are the volume fraction and average size of carbides, respectively. The precipitation particles in automobile steels coiled at different temperatures were mainly (Ti, V)C carbides. As carbides in different size and volume fraction contributed different strengthening effect, it is hard to quantify the precipitation strengthening due to the totally different size and volume fraction of (Ti, V)C carbides in the two specimens. The precipitation strengthening was approximated by calculating the difference between the measured yield strength and the sum of all other identified strength contributions. Similar methods have been applied in many existing research [35-36]. As a result, the estimated precipitation strengthening values for the specimens coiled at 400°C and 600°C were 311.09 MPa and 293.53 MPa, respectively.

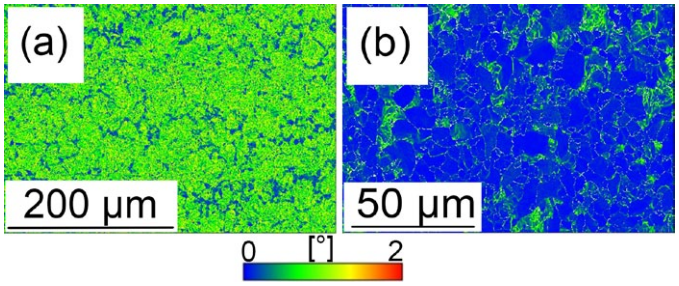

Fig. 11. Kernel Average Misorient distribution of specimens coiled at (a) 400 and (b) 600°C

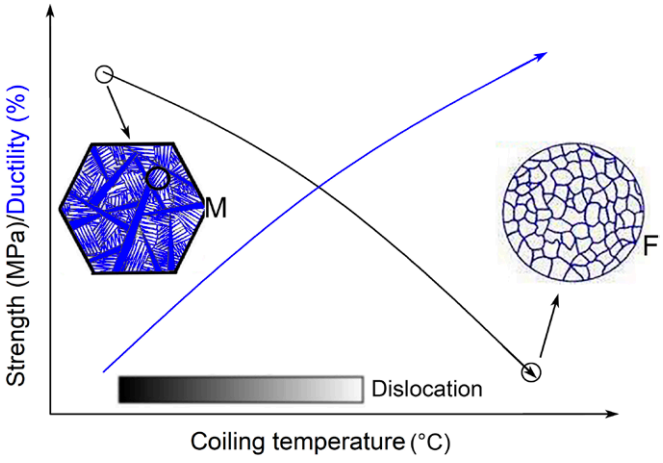

Fig. 12. Schematic diagram showing the microstructure evolution with the increasing coiling temperature

$$\Delta\sigma_p = \frac{0.538 G b f^{\frac{1}{2}}}{d} \ln\frac{d}{2b} \tag{6}$$

TABLE 1 gives the calculation of strength contributions in automobile steels coiled at different temperatures. The primary differences in strength observed between specimens coiled at varying temperatures were attributed to phase transformation strengthening, grain refinement strengthening, dislocation strengthening, and precipitation strengthening. Notably, the phase transformation strengthening and dislocation strengthening emerged as the predominant factors contributing to these strength variations. The martensite microstructure dominated the higher strength compared to the ferrite although its size was relatively larger. The conspicuous difference in dislocation strengthening was ascribed to the enhanced dislocation annihilation at the higher coiling temperature. Besides, the formed small-sized (Ti, V)C carbides in the specimen coiled at 400°C contributed to hindering the dislocation migration.

TABLE 1

Strength contributions in lightweight steels coiled at 400 and 600°C

Coiling temperature (°C)	σ_0	σ_{tran}	$\Delta\sigma_s$	$\Delta\sigma_g$	$\Delta\sigma_\rho$	$\Delta\sigma_p$	σ
400	48	54.8	96.68	83.67	185.86	311.09	780.10
600	48	0	96.68	95.97	114.72	293.53	648.90

In a word, the automobile steel with low Mn-Al content was fabricated in current work. The optimal balance between tensile strength and ductility were 897.7 MPa and 19.3% when coiled at 400°C. Fig. 12 manifests the microstructure evolution in the automobile steel coiled from 400 to 600°C. The intrinsic factors caused the decreased strength when coiling at higher temperature were the annihilating dislocation and ferrite transformation. Results in current work indicate that the automobile steel with low Mn-Al content and decreased density could be produced just by hot rolling process. Different with some reported lightweight steels with large amount Mn-Al, the chemical composition and corresponding hot rolling process in current work are easily acceptable for industrial production due to few difficulties in smelting and continuous casting. More important, the decreased density and fair mechanical properties could be simultaneously realized.

5. Conclusion

(1) One novel Fe-1.5Al-2Mn-0.18C automobile steel with 897.7 MPa tensile strength and 19.3% ductility was fabricated. The decreased density and fair mechanical properties could be simultaneously realized by hot rolling process.

(2) The variation in strength caused by differing coiling temperatures was primarily due to four factors: phase transformation strengthening, grain refinement strengthening, dislocation strengthening, and precipitation strengthening. Among these, phase transformation strengthening and dislocation strengthening were the dominant contributors.

(3) The size and volume fraction of (Ti, V)C particles both decreased with the decrease in coiling temperature, which was related to the different carbides ripening and nucleation behavior under the different coiling temperature.

Acknowledgments

The authors gratefully acknowledge the financial supports from the Competitive Scientific and Technological Research Projects of Quzhou Science and Technology Bureau (2024K180), Guiding Scientific and Technological Research Projects of Quzhou Science and Technology Bureau (Y202455648) and the Nature Science Foundation of Hubei Province (No. 2024AFB900).

REFERENCE

[1] S. Lee, J. Moon, H. Kim, Y. H. Cho, H.H. Lee, H. Choi, Y. Kim, D.W. Suh, K. Jeong, H.N. Han, Mater. Sci. Eng. A. **891**, 146003 (2024).

[2] L. Liu, Y. Zhao, W.N. Li, X.L. Xu, Z.Z. Zhao, Mater. Charact. 113787 (2024). doi: 10.1016/j.matchar.2024.113787

[3] Y. Xiong, Z.W. Luan, N. Du, Y. Li, X.J. Du, T.T. He, F.Z. Ren, S.B. Wang, Mater. Charact. 113788, (2024). DOI: https://doi.org/10.1016/j.matchar.2024.113788

[4] U.S. Ko, C. Kim, S.J. Park, H.U. Hong, Int. J. Fatigue **181**, 108149 (2024).

[5] K. Sairam, M.P. Phaniraj, K. Rajesh, Scripta Mater. **230**, 115399 (2023).

[6] Y.H. Tang, P.F. Ji, B. Li, G.F. Zhang, W. Ma, F. Wang, X.Y. Zhang, M.Z. Ma, R.P. Liu, Tribol. Int. **177** (2023). DOI: https://doi.org/10.1016/j.triboint.2022.108006

[7] J.H. Shin, J.Y. Song, S.D. Kim, S.J. Park, Y.W. Ma, J.W. Lee, Materials **15**, 8909-8921 (2022).

[8] S. Khaple, B.R. Golla, V.V. Satya Prasad, Def. Technol. **26**, 1-22 (2022).

[9] M. Harwarth, G. Chen, R. Rahimi, H. Biermann, A. Zargaran, M. Duffy, M. Zupan, J. Mola, Mater. Design. **206**, 109813 (2021).

[10] D. Kumar, R.K. Phanden, L. Thakur, Mater. Today: Proc. **38**, 359-364 (2021).

[11] J. Lee, H. Kim, K. Jeong, S.J. Park, J. Moon, S. Kang, H.N. Han, J. Mater. Res. Technol. **14**, 2897-2908 (2021).

[12] Z.H. Lai, Y. Sun, Y.T. Lin, J.F. Tu, H.W. Yen, Acta Mater. **210**, 116814 (2021).

[13] P. Chen, F. Zhang, Q.C. Zhang, J.H. Du, F. Shi, X.W. Li, J. Mater. Res. Technol. **25**, 3780-3788 (2023).

[14] Y.H. Tang, B. Li, H.Y. Shi, Y.X. Guo, S.Z. Zhang, J.S. Zhang, X.Y. Zhang, R.P. Liu, Mater. Charact. **205**, 113274 (2023).

[15] S. Picak, M.W. Vaughan, O. El Atwani, A. Mott, K.R. Limmer, I. Karaman, Acta Mater. **245**, 118589 (2023).

[16] W. Peng, X.Q. Gao, X.F. Guo, H.C. Lu, G.S. Li, X.S. Xiao, D.X. Xu, X.C. Wei, H. Dong, Mater. Design. **196**, 109163 (2020).

[17] J. Jeong, C.Y. Lee, I.J. Park, Y.K. Lee, J. Alloys and Compd. **574**, 299-304 (2013).

[18] Z.H. Cai, H. Ding, R.D.K. Misra, S.Q. Qiguang, Mater. Sci. Eng. A. **652**, 205-211 (2016).

[19] Z.H. Cai, H. Ding, H.Y. Li, M.L. Huang, F.R. Cao, Mater. Sci. Eng. A. **6584**, 150-155 (2013).

[20] H. Kim, D.W. Suh, N.J. Kim. Sci. Technol. Adv. Mat. **14**, 014205 (2013).

[21] Q.X. Zhang, Q, Yuan, Z.Q. Xiong, M. Liu, G. Xu. Phys. Met. Metallogr. **122**, 1463-1472 (2021).

[22] J.S. Guan, Q, Yuan, Z.Q. Xiong, Q.X. Zhang, G. Xu. Mater. Res. Express. **7**, 016536-016536 (2019).

[23] H.J. Hu, H.S. Zurob, G. Xu, D. Ernbury, G.R. Purdy. Metall. Mater. Trans. A. **626**, 34-40 (2014).

[24] Q. Yuan, Z.B. Li, Q.X. Zhang, G. Xu, Mater. Sci. Eng. A. **886**, 145674 (2023).

[25] Y.H. Wang, Study on microstructure, mechanical properties and heat treatment of Fe-12.6Mn-9Al-0.8C low density cast steel[D]. Hebei University of Technology, Master thesis, 2015.

[26] S.C. Li. Control of microstructure and mechanical properties of high aluminum low silicon high strength automobile steel[D]. Northeastern University, Master thesis, 2018.

[27] S.S. Sohn, Lee B J, Lee S, N.J. Kim, J.H. Kwak, Acta Mater. **61**, 5050-5066 (2013).

[28] L. Kucerova, K. Burdova, A. Stehlik, I. Ticha, 5th PING Junior Conference: Modern Trends in Material Engineering, IOP Conf. Series: Materials Science and Engineering **1161**, 012002 (2021).

[29] Z.C. Li, Y.J. Mou, X.J. Li, R.D.K. Misra, L.F. He, H.P. Li, J. Mater. Eng. Perform. **29**, 4396-4403 (2020).

[30] Z.C. Li, X.T. Zhang, Y.J. Mou, Z.H. Cai, R.D.K. Misra, L.F. He, H.P. Li, H. Ding, Mater. Sci. Technol. **36**, 500-510 (2020).

[31] X.L. Gan, Q. Yuan, G. Zhao, H.W. Ma, W. Liang, Z.L. Xue, W.W. Qiao, G. Xu, Metall. Mater. Trans. A. **51**, 2084-2096 (2020).

[32] Q. Yuan, J. Ren, J.X. Mo, Z.C. Zhang, E. Tang, G. Xu, Z.L. Xue. J. Mater. Res. Techno. **23**, 3756-3771 (2023).

[33] Z.B. Li, Q. Yuan, S.P. Xu, Y. Zhou, S. Liu, G. Xu, Materials **16**, 3840-3857 (2023).

[34] X.L. Gan, Q.Yuan, G. Zhao, H.J. Hu, J.Y. Tian, G. Xu. Steel Res. Int. **90**, 1-9 (2019).

[35] E. Tang, Q. Yuan, R. Zhang, J. Ren, Z.B. Li, G. Xu. J. Mater. Res. Technol. **30**, 2596-2608 (2024).

[36] Q. Yuan, J.X. Mo, J. Ren, W. Liang, G. Xu. J. Mater. Res. Technol. **31**, 264-275 (2024).